

Picosecond IR–UV pump–probe spectroscopic study of the dynamics of the vibrational relaxation of jet-cooled phenol. II. Intracluster vibrational energy redistribution of the OH stretching vibration of hydrogen-bonded clusters

Masakazu Kayano, Takayuki Ebata,^{a),b)} Yuji Yamada, and Naohiko Mikami^{a)}

Department of Chemistry, Graduate School of Science, Tohoku University, Sendai, 980-8578, Japan

(Received 30 October 2003; accepted 20 January 2004)

A picosecond time-resolved IR–UV pump–probe spectroscopic study has been carried out for investigating the intracluster vibrational energy redistribution (IVR) and subsequent dissociation of hydrogen-bonded clusters of phenol (C_6H_5OH) and partially deuterated phenol (C_6D_5OH , phenol- d_5) with various solvent molecules. The H-bonded OH stretching vibration was pumped by a picosecond IR pulse, and the transient S_1-S_0 UV spectra from the pumped level as well as the redistributed levels were observed with a picosecond UV laser. Two types of hydrogen-bonded clusters were investigated with respect to the effect of the H-bonding strength on the energy flow process: the first is of a strong “ σ -type H-bond” such as phenol-(dimethyl ether) $_{n=1}$ and phenol dimer, and the second is phenol-(ethylene) $_{n=1}$ having a weak “ π -type H-bond.” It was found that the population of the IR-pumped OH level exhibits a single-exponential decay, whose rate increases with the H-bond strength. On the other hand, the transient UV spectrum due to the redistributed levels showed a different time evolutions at different monitoring UV frequency. From an analysis of the time profiles of the transient UV spectra, the following three-step scheme has been proposed for describing the energy flow starting from the IVR of the initially excited H-bonded OH stretching level to the dissociation of the H bond. (1) The intramolecular vibrational energy redistribution takes place within the phenolic site, preparing a hot phenol. (2) The energy flows from the hot phenol to the intermolecular vibrational modes of the cluster. (3) Finally, the hydrogen bond dissociates. Among the three steps, the rate constant of the first step was strongly dependent on the H-bond strength, while the rate constants of the other two steps were almost independent of the H-bond strength. For the dissociation of the hydrogen bond, the observed rate constants were compared with those calculated by the Rice, Ramsperger, Kassel, and Marcus model. The result suggests that dissociation of the hydrogen bond takes place much faster than complete energy randomization within the clusters. © 2004 American Institute of Physics. [DOI: 10.1063/1.1668641]

I. INTRODUCTION

The vibrational relaxation of the OH stretching vibration has long been investigated by many researchers because of the importance of the OH group in nature and it is the fundamental process in the liquid phase. Up to now many experiments have been carried out, mostly time-resolved spectroscopic studies,^{1–17} to elucidate the dynamics of the OH stretching vibration. In the liquid phase, it has been known that vibrational excitation leads to a rapid dissociation of the H-bond, followed by a rather slow recombination. However, as to the energy flow mechanism from the OH stretch to the H-bond dissociation, the issue is still open whether the energy of the OH stretch directly flows into the intermolecular H-bonding coordinate^{2,3,5} or flows sequentially via intramolecular vibrational modes.^{10,12–14}

The recent development of double-resonant vibrational spectroscopy combined with supersonic jets has enabled us to measure the spectra of the OH stretching vibrations of

size-and-structure-selected H-bonded clusters.^{18–34} It has been found that the IR spectra of the OH stretching vibration of such H-bonded clusters with solvent molecules exhibit a very similar feature with that observed in the corresponding condensed phase. In spectroscopic studies of jets, the cluster structures can be determined from an analysis of the observed spectra with the aid of *ab initio* molecular orbital or density functional calculations. Thus we are in the stage where we can study in detail the dynamics of the H-bonded OH stretching vibration for the well-characterized H-bonded system.

In this work, the second paper of the series, we report a picosecond IR–UV pump–probe study of the intracluster vibrational energy redistribution (IVR) and subsequent dissociation of H-bonded clusters of phenol and partially deuterated phenol (phenol- d_5), after IR excitation of the OH stretching vibration. Very recently, we reported our first work on the picosecond dynamics of the OH stretching vibration of phenol and its H-bonded clusters.³⁵ We could show that the IVR lifetime of the donor OH stretch is substantially shortened upon H-bonding, while that of the acceptor OH stretch was similar to bare phenol. However, a detailed

^{a)}Authors to whom correspondence should be addressed.

^{b)}Electronic mail: ebata@qclhp.chem.tohoku.ac.jp

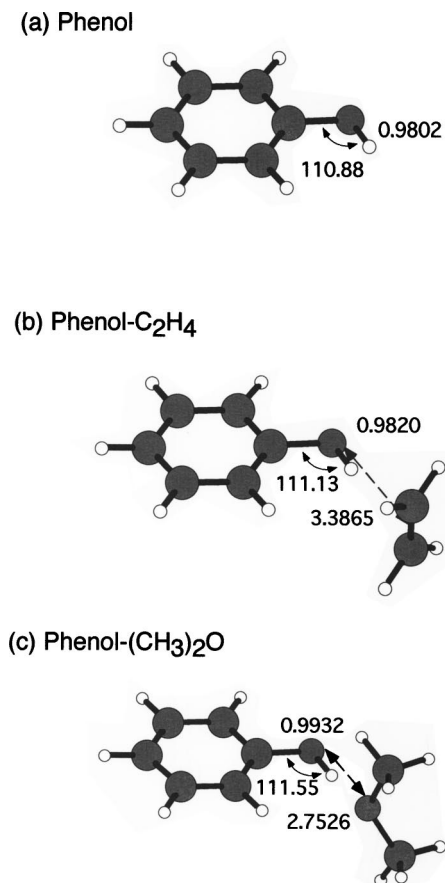


FIG. 1. *Ab initio* calculated structures of phenol, phenol-C₂H₄, and phenol-(CH₃)₂O at the MP2/6-31G level. The numbers are C–O–H bond angle (degree), OH bond length (Å), and distance (Å) between the phenolic OH oxygen atom and the center of C=C bond of C₂H₄ or an oxygen atom of (CH₃)₂O.

mechanism of the energy flow and the effect of the H-bonding strength are still unknown.

The aim of the present work is to reveal the energy flow pathway starting from the OH stretch vibration to the dissociation of the H-bond. We have picked up two types of H-bonded clusters whose binding energies are quite different. First is the π -type H-bonded cluster, which is phenol-(ethylene)_{*n*=1}, and the second is the σ -type H-bonded cluster, which is phenol-[dimethyl ether (DME)]_{*n*=1}. Their calculated structures are shown in Fig. 1. Phenol-(ethylene)_{*n*=1} has a weak π -type H-bond between phenolic OH and the π electron of ethylene. Though the binding energy of the “OH- π ” bond has not been experimentally obtained, high-level *ab initio* calculations predict the energy to be 900–1100 cm⁻¹.^{36–39} On the other hand, phenol-(DME)_{*n*=1} has a strong σ -type H bond between phenolic OH and Oxygen of DME. The H-bond energy of phenol-(DME)_{*n*=1} is estimated to be 2000–2100 cm⁻¹ from an analogy with the other H-bonded clusters of phenol.⁴⁰ We will see how the H-bond strength affects the energy flow mechanism and its rate constant. The entire investigation is based on the observation of time-resolved transient UV spectra and time profiles of the pump-probe signals.

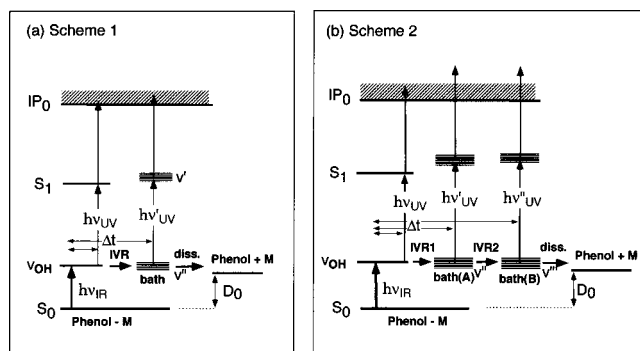


FIG. 2. Energy diagram and two relaxation schemes: (a) single-bath-mode scheme and (b) sequential two-bath-mode scheme.

II. EXPERIMENT

Figure 2 shows the excitation scheme of picosecond IR–UV pump–probe spectroscopy. Two relaxation schemes are shown, which will be discussed later. Essentially, the OH stretching vibration of the phenol or phenol-(solvent molecule)_{*n*=1} H-bonded cluster is pumped by a picosecond IR laser pulse, and at several delay times a picosecond UV laser pulse is introduced to measure the (1+1) resonance-enhanced multiphoton ionization spectra through the S₁ state, which correspond to the transient UV spectra. The time evolution of the IR-laser-pumped OH level is observed with the OH₁⁰ band, while those of the levels (*v*′) generated by IVR are observed by the *v*′ ← *v*″ transition. The spectrum of the latter transition exhibits a broad feature due to the overlap of many transitions of vibrational levels (*v*′) generated by the IVR: hereafter, we call those levels “IVR levels.”

A detailed description of the experimental setup of picosecond IR–UV pump–probe spectroscopy was given in paper I of this series. A picosecond tunable UV pulse was obtained by frequency doubling the mode-locked picosecond Nd³⁺:YAG laser (Ekspra PL2143B) pumped OPG/OPA output (Ekspra PG401SH). A tunable picosecond IR pulse was generated by a homemade OPG/OPA system pumped by the same mode-locked Nd³⁺:YAG laser. The spectral resolution was estimated to be 10 and 15 cm⁻¹ for the UV and IR laser lights, respectively. The pulse widths of the pump and probe laser pulses were determined to be 14 ps, by fitting the time profile of the IR–UV pump–probe signal of the CH stretching vibration of benzene.

Jet-cooled phenol and its clusters were generated by a supersonic expansion of phenol vapor seeded in ethylene (2%)/He or dimethyl ether (0.5%)/He mixed carrier gas at a total pressure of 3 atm into vacuum through a pulsed nozzle (General valve) having a 0.8-mm aperture. Phenol was heated up to 40 °C. Phenol and its H-bonded clusters in the jet were skimmed by a skimmer (0.8 mm-diam beam dynamics) located at 30 mm downstream of the nozzle. The IR and UV lasers were introduced into a vacuum chamber in a counterpropagated manner and crossed the supersonic beam at 50 mm downstream of the skimmer. The molecules in the supersonic beam were ionized by (1+1) resonance-enhanced multiphoton ionization (REMPI) via S₁, and the ions were

repelled to a direction perpendicular to the plane of the molecular beam and laser beams. The ions were then mass analyzed by a 50-cm time-of-flight tube and were detected by an electron multiplier (Murata Ceratron). The transient profiles of the pump–probe ion signals were observed by changing a delay time between UV and IR pulses by a computer-controlled optical delay line. The ion signals were integrated by a boxcar integrator (Par model 4420/4400) and were processed by a microcomputer.

We should comment on the effect of the larger-size clusters—that is, phenol-(solvent molecule)_{*n*>1}—in the present work. First of all, we have chosen the solvent molecules, ethylene and dimethyl ether, which form exclusively 1:1 H-bonded clusters. This is because once the 1:1 H-bonded cluster is formed, as can be expected from Fig. 1, the next solvent molecule will be bound via a much weaker van der Waals force. Actually, the signal intensities of larger-size clusters were negligibly small in the time-of-flight spectra. So perturbation of the larger-size clusters, such as the formation of smaller-size cluster ions after the ionization, is thought to be very small. In addition, the larger-size clusters may have OH stretching frequencies different from the 1:1 cluster. Another point is the effect of the dissociation of the 1:1 clusters after the ionization. The binding energies of the 1:1 clusters studied in the present work are not precisely known and it is quite possible that the cluster will dissociate after the one-color 1 + 1 ionization. Actually we observed the phenol fragment ion in the IR-pump–UV-probe experiment at the higher monitoring UV frequencies. Then we observed the pump–probe time profile by monitoring both the parent cluster ion and the phenol fragment ion. As a result, we obtained the same time profile between them. So we concluded that observation of the 1:1 cluster ion is good enough for the present study.

Phenol (99.0%) was purchased from Wako Chemical Ind. Ltd. and was purified by vacuum sublimation before use. Phenol-*d*₅(C₆D₅OH) was synthesized by adding a few drops of water to phenol-*d*₆(C₆D₅OD, 98 at. % D) purchased from Sigma-Aldrich Fine Chemicals. C₂H₄ was purchased from Nippon Sanso, and DME was purchased from Wako Chemical Ind. Ltd.

III. RESULTS

A. IR spectra

Figure 3 shows the IR spectra of (a) phenol and its H-bonded clusters with (b) C₂H₄ and (c) dimethyl ether (DME) in the 2800–3700 cm⁻¹ region. All spectra are obtained as the ion-gain IR spectra. The UV laser pulse was introduced at a delay time of 40 ps after IR pulse excitation, and the IR frequency was scanned while monitoring the broad transition due to the IVR levels. In bare phenol [Fig. 3(a)], the band at 3657 cm⁻¹ is the OH stretching vibration and many bands in 3000–3100 cm⁻¹ are due to CH stretching vibrations. In the IR spectrum of phenol–C₂H₄, the H-bonded OH stretching vibration appears at 3580 cm⁻¹. The relatively small redshift (77 cm⁻¹) of the OH stretch with respect to the bare phenol represents a typical feature of the π -type H-bond.³⁴ Two intense bands at 2987 and 3104

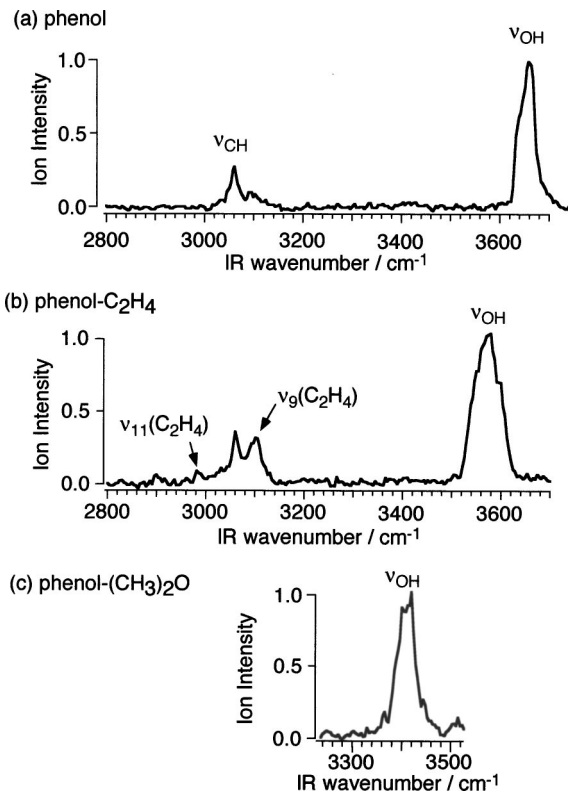


FIG. 3. Ionization-detected IR spectra of (a) phenol, (b) phenol–C₂H₄, and (c) phenol–(CH₃)₂O ether in the OH and CH stretching regions. The delay time between the IR and UV pulses was set to 40 ps, and the UV frequencies were fixed to the electronic transition from the vibrational levels generated by IVR.

cm⁻¹ are the CH stretching vibrations of the C₂H₄ site. The appearance of those bands indicates that the IVR also occurs in those vibrations in this time scale. The dynamics of those bands will be discussed in a separate paper. The H-bonded OH stretch of phenol–DME in Fig. 3(c) appears at 3410 cm⁻¹. A lower-frequency shift as large as 250 cm⁻¹ is much larger than that of phenol–ethylene. The IR spectra for phenol-*d*₅–C₂H₄ and –DME were very similar to those of phenol–C₂H₄ and –DME, respectively, and the obtained frequencies of the OH stretching vibration were the same within our experimental uncertainty. In the following, we examine the dynamics for these vibrations by measuring the time-resolved UV spectra.

B. Vibrational relaxation of the H-bonded OH stretch of phenol–C₂H₄

Figure 4 shows the transient UV (1 + 1 REMPI) spectra of phenol–C₂H₄ measured at several delay times after IR excitation of the H-bonded OH stretch vibration at 3580 cm⁻¹. Each spectrum is shown in the manner that the 1 + 1 REMPI spectrum measured without the IR laser irradiation is subtracted. In the figure, the OH₁⁰ band (32 500 cm⁻¹) and sharp vibronic bands are seen at short delay times, such as at $\Delta t = 3$ and 26 ps. In addition, a broad continuum transition appearing from 34 000 cm⁻¹ to the higher-frequency side is also seen, which is attributed to the transition from the IVR levels. The broad continuum transition disappears at long

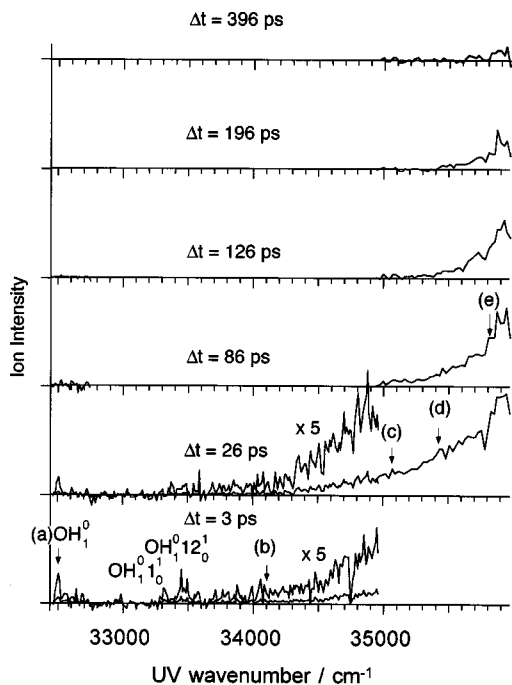


FIG. 4. Transient 1 + 1 REMPI spectra of phenol-C₂H₄ measured at several delay times after IR pulse excitation of the H-bonded OH stretching vibration. Each spectrum is shown in the manner that the 1 + 1 REMPI spectrum measured without IR light irradiation is subtracted.

delay times, such as $\Delta t = 396$ ps, because of the H-bond dissociation of the cluster. Very interestingly, we found that the relative intensity of the different regions of the continuum spectra changes with time. For example, when we compare the intensity pattern of the broad transient UV spectra between $\Delta t = 26$ and 86 ps, we see that the intensity ratio of the low-frequency region ($\nu_{UV} < 35\,500$ cm⁻¹) to the high-frequency region ($\nu_{UV} > 35\,500$ cm⁻¹) is much smaller at $\Delta t = 86$ ps than that at $\Delta t = 26$ ps. The result represents that the lower-frequency part of the transient continuum spectrum decays faster than that of the high-frequency part.

In order to have clear evidence, we measured the time profiles of the pump-probe signals at different UV frequencies, which are marked by arrows in Fig. 4. The results are shown in the traces (a)–(e) in Fig. 5. First, the decay curve of the OH₁⁰ band [Fig. 5(a)] could be fitted by a single-exponential decay with a lifetime of $\tau_{IVR} = 10$ ps, corresponding to an IVR rate constant of 1.0×10^{11} s⁻¹. Since the lifetime of the OH stretch of bare phenol has already been obtained to be 7.1×10^{10} s⁻¹, we see the π -type H-bonding slightly accelerates the IVR rate of the OH stretch.

In accordance with the complicated features of the transient UV spectra as mentioned above, the time evolution of the IVR levels shows different profiles at different monitoring UV frequencies. That is, the time evolution observed at lower UV frequencies shows both faster rises and faster decays than those monitored at higher UV frequencies. For example, the pump-probe signal observed at $\nu_{UV} = 34\,110$ cm⁻¹ [Fig. 5(b)] reaches a maximum intensity at $\Delta t = 20$ ps and disappears at $\Delta t = 90$ ps. As shown in Fig. 5(e), on the other hand, the signal monitored at $\nu_{UV} = 35\,820$ cm⁻¹ reaches the maximum intensity at Δt

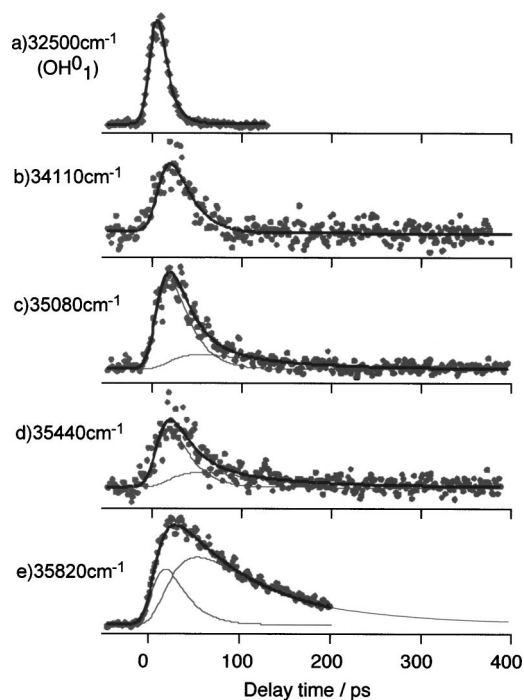


FIG. 5. Time profiles of the IR-UV pump-probe signals of phenol-C₂H₄ measured at several UV frequencies. The thick solid curves are the fitted curves by using Eqs. (1a)–(1c). The dotted curves are the calculated time profiles of bath states A and B, respectively. The calculation has been performed by assuming Gaussian curves for the pump and probe pulses with pulse widths of 14 ps. See text.

$= 30$ ps and diminishes at a delay time of a few hundreds picoseconds. The result evidently indicates that we are observing different portions of the IVR levels when we monitor different parts of the UV spectrum, and they exhibit different time evolutions from each other.

C. Phenol-DME

The upper part of Fig. 6 shows the transient UV spectra observed at several delay times after exciting the OH stretching vibration at 3410 cm⁻¹, and the lower part of Fig. 6 shows the pump-probe time profiles observed at three different UV frequencies. First, the OH₁⁰ band at $32\,500$ cm⁻¹ decays very rapidly and its lifetime was obtained to be equal to or less than 5 ps, which is the shortest lifetime obtained with the present laser system. The corresponding IVR rate constant of $k_{IVR} \geq 2.0 \times 10^{11}$ s⁻¹ is more than two times larger than that of phenol-C₂H₄. On the other hand, the temporal behavior of the broad transient UV spectrum and the time profiles of the pump-probe signals show a very similar feature with those of phenol-C₂H₄: that is, as seen in the transient UV spectra in Fig. 6, the low-frequency part ($\nu_{UV} < 35\,000$ cm⁻¹) of the broad transition diminishes faster than the high-frequency part ($\nu_{UV} > 35\,000$ cm⁻¹). Accordingly, in the lower part of Fig. 6, the time profile monitored at $\nu_{UV} = 34\,100$ cm⁻¹ of the broad transition exhibits a faster rise as well as a rapid decay in comparison with that observed at $\nu_{UV} = 35\,500$ cm⁻¹, indicating a similar energy flow mechanism with that of phenol-C₂H₄.

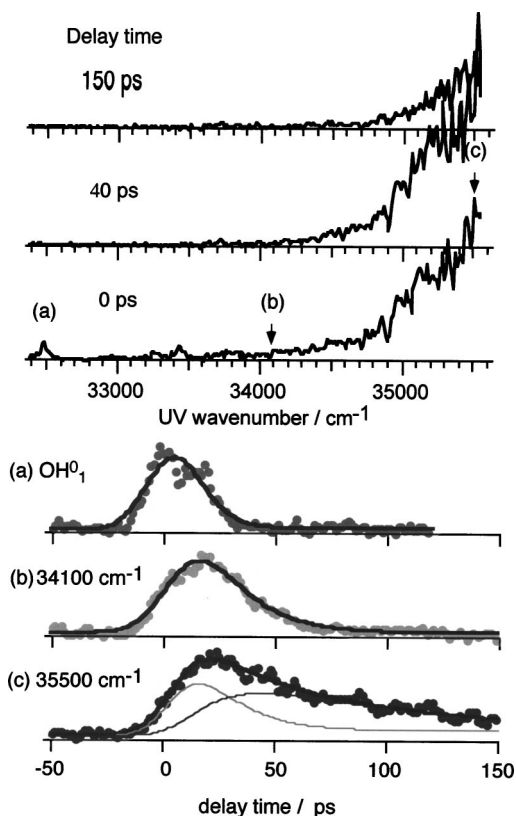


FIG. 6. (Upper) Transient 1+1 REMPI spectra of phenol-(CH₃)₂O measured at several delay times after IR pulse excitation of the H-bonded OH stretching vibration. Each spectrum is shown in the manner that the 1+1 REMPI spectrum measured without IR light irradiation is subtracted. (Lower) Time profiles of the IR-UV pump-probe signals measured at several UV frequencies. The solids curves are the best-fitted curves by using Eqs. (1a)–(1c) and assuming Gaussian curves for the pump and probe pulses with pulse widths of 14 ps.

D. Phenol-*d*₅-C₂H₄ and -DME

Similar experiments have been carried out for the H-bonded clusters of phenol-*d*₅. Figures 7 and 8 show transient 1+1 REMPI spectra and the pump-probe profiles after picosecond IR pulse excitation of the H-bonded OH stretch vibration of phenol-*d*₅-C₂H₄ and -DME, respectively. In paper I of this series, we reported the IVR rate constant of the OH stretching vibration of bare phenol-*d*₅ to be $1.3 \times 10^{10} \text{ s}^{-1}$. The IVR rate constant has changed to $6.7 \times 10^{10} \text{ s}^{-1}$ and $1.4 \times 10^{11} \text{ s}^{-1}$ upon the H-bonding with C₂H₄ and DME, respectively. On the other hand, the transient UV spectra and time profiles of the pump-probe signal showed very similar features with those of the corresponding H-bonded clusters of phenol. Thus it is concluded that the same relaxation mechanism is held in all H-bonded clusters examined.

IV. DISCUSSION

A. Analysis of the time evolution and a mechanism of energy redistribution in the clusters

As was shown above, we found that the different portions of the IVR levels (bath mode) exhibit different time evolutions. The result indicates that the energy flow starting

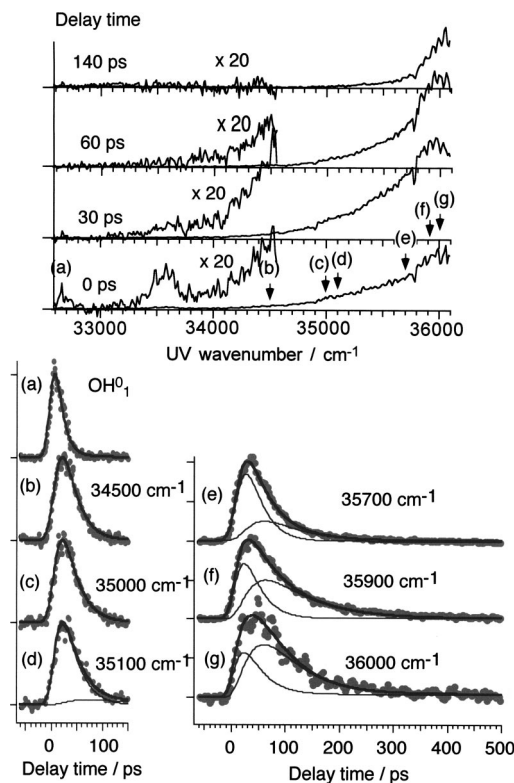


FIG. 7. (Upper) Transient 1+1 REMPI spectra of phenol-*d*₅-C₂H₄ measured at several delay times after IR pulse excitation of the H-bonded OH stretching vibration. Each spectrum is shown in the manner that the 1+1 REMPI spectrum measured without IR light irradiation is subtracted. (Lower) Time profiles of the IR-UV pump-probe signals measured at several UV frequencies. The solids curves are the best-fitted curves by using Eqs. (1a)–(1c) and assuming Gaussian curves for the pump and probe pulses with pulse widths of 14 ps.

from the OH stretch level to the dissociation of the H bond cannot be explained by a simple two-step process with a single bath mode—that is, scheme (1) in Fig. 2(a). According to this scheme, the IVR level (bath mode) would exhibit the

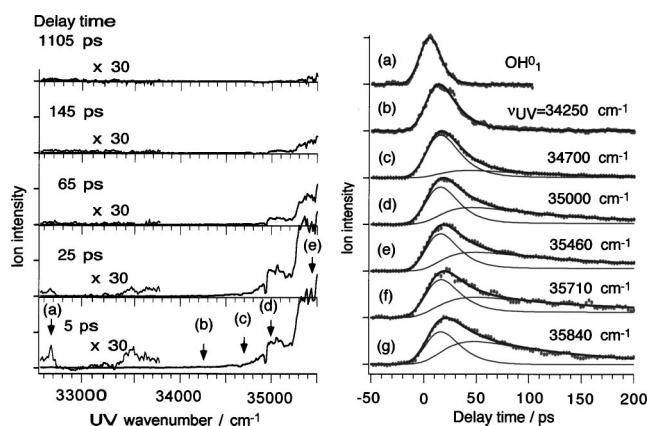


FIG. 8. (Left) Transient 1+1 REMPI spectra of phenol-*d*₅-(CH₃)₂O measured at several delay times after IR pulse excitation of the H-bonded OH stretching vibration. Each spectrum is shown in the manner that the 1+1 REMPI spectrum measured without IR light irradiation is subtracted. (Right) Time profiles of the IR-UV pump-probe signals measured at several UV frequencies. The solids curves are the best-fitted curves by using Eqs. (1a)–(1c) and assuming Gaussian curves for the pump and probe pulses with pulse widths of 14 ps.

TABLE I. IR frequencies of the OH stretching vibration ν_{OH} , redshift by the H bonding, Δ , the H-bond dissociation energies D_0 , the observed rate constants k_1 , k_2 , and k_3 , and the calculated dissociation rate constants k_{RRKM} using the RRKM model.

	ν_{OH} (cm ⁻¹)	Δ (cm ⁻¹)	D_0 (cm ⁻¹)	k_1 ($\times 10^{10}$ s ⁻¹)	k_2 ($\times 10^{10}$ s ⁻¹)	k_3 ($\times 10^{10}$ s ⁻¹)	k_{RRKM} ($\times 10^{10}$ s ⁻¹)
Phenol	3657	-	-	7.1	-	-	-
Phenol-C ₂ H ₄	3580	77	1100 ^b	10	5.0	1.1	18
Phenol dimer	3530 ^a	127	2100 ^b	$\geq 20^c$	^c	1.3 ^c	0.10
Phenol-DME	3410	247	2100 ^b	≥ 20	5.0	1.1	0.045
Phenol- <i>d</i> ₅	3657	-	-	1.3	-	-	-
Phenol- <i>d</i> ₅ -C ₂ H ₄	3580	77	-	6.7	4.0	1.2	-
Phenol- <i>d</i> ₅ -DME	3410	247	-	14	4.0	0.91	-

^aDonor OH stretching vibration.

^bEstimated binding energies for obtaining k_{RRKM} . See text.

^cThough the detailed analysis based on Eq. (1) has not been preformed, k_1 was obtained from the decay of the OH₁⁰ band, and k_3 was obtained from the time profile of the broad band measured at the UV frequency close to the band origin.

same time profile independent of the monitoring portion. Instead, we constructed the “sequential two-bath-mode model”—that is, scheme (2) of Fig. 2(b). In this model, the population of the OH stretching level is first redistributed to “bath mode (A)” with a rate constant k_1 ($= 1/\tau_{\text{IVR1}}$), followed by a further redistribution into “bath mode (B)” with a rate constant k_2 ($= 1/\tau_{\text{IVR2}}$). Finally, the clusters in “bath mode (B)” dissociate with a rate constant k_3 ($= 1/\tau_{\text{diss}}$). The time profiles of the OH stretch vibration, $I_{\text{OH}}(t)$, bath mode (A), $I_{\text{bath(A)}}(t)$, and bath mode (B), $I_{\text{bath(B)}}(t)$, are expressed as

$$I_{\text{OH}}(t) = C_0 e^{-k_1 t}, \quad (1a)$$

$$I_{\text{bath(A)}}(t) = C_{\text{bA}} (-e^{-k_1 t} + e^{-k_2 t}), \quad (1b)$$

$$I_{\text{bath(B)}} = C_{\text{bB}} \{ (k_2 - k_3) e^{-k_1 t} + (k_3 - k_1) e^{-k_2 t} + (k_1 - k_2) e^{-k_3 t} \}. \quad (1c)$$

The rate constant k_1 has been already obtained from the decay curve of the OH₁⁰ band. On the other hand, the rate constants k_2 and k_3 cannot be obtained from a decay curve at a single UV frequency, because the electronic transitions of both bath modes (A) and (B) would overlap in the broad transient UV spectra. In this sequential model, the population of bath A is transferred to bath mode (B), so that $I_{\text{bath(A)}}(t)$ will reach the maximum earlier, and decays faster than those of $I_{\text{bath(B)}}(t)$, respectively. On the other hand, the pump-probe signals observed at the low-frequency region of the broad continuum showed a faster rise and decay than that observed at the high-frequency region. Consequently, bath mode (A) is thought to contribute mostly to the low-frequency region of the transient UV spectra, while bath mode (B) to the high-frequency region. Actually, the two components are not separated in the spectra as mentioned above, and the observed curves are expressed by the sum of the two components $I_{\text{bath(A)}}$ and $I_{\text{bath(B)}}$. We carried out least-squares fitting to the observed curves by changing the parameters k_2 , k_3 , and the ratio $C_{\text{bA}}/C_{\text{bB}}$, where $C_{\text{bA}}/C_{\text{bB}}$ differs at different UV frequencies. The best-fitted curves are also shown as solid curves in Figs. 5–8, and the rate constants obtained by the best fitting are listed in Table I.

Before discussing the obtained rate constants in Table I, we have to mention a clear picture of bath modes (A) and (B). In Figs. 3 and 5–8, the broad continuum observed at

short delay times extends more than 2000 cm⁻¹ below the band origins. Such large redshifted hot bands cannot be the hot band transitions of the intermolecular modes, because the vibrational frequencies of intermolecular modes are less than 200 cm⁻¹ (Refs. 41 and 42) so that the Franck–Condon factors involving large vibrational quanta of those modes for such largely redshifted transitions (2000 cm⁻¹) should be negligibly small. Thus the broad continuum observed at short delay times is attributed to the hot band transitions of intramolecular modes of the phenolic site, whose frequencies are much higher than those of the intermolecular modes. The result means that bath mode (A) corresponds to the intramolecular modes of the phenolic site, and we conclude that the OH stretching vibrational energy is initially redistributed mostly into the phenolic mode, but not into the intermolecular modes.

With an increase of the delay time, the low-frequency region of the broad continuum diminishes rapidly, while the high-frequency region still remains. At long delay times, the vibrational energy in the phenolic site is thought to be redistributed into the intermolecular modes, which corresponds to bath mode (B). Since the vibrational frequencies of the intermolecular modes are low, their vibronic transitions would appear closely to the band origin. This is the reason why the higher-frequency part of the broad electronic transition remained at longer delay times. Finally, the clusters in bath mode (B) dissociate with the rate constant k_3 .

From the above discussion, we propose a model of the whole relaxation process starting from the phenolic OH stretching vibration; the energy of the OH stretch is first redistributed mostly to the intramolecular bath mode (A) of the phenolic site with rate constant k_1 , and the energy of bath mode (A) further relaxes to intermolecular bath mode (B) with rate constant k_2 . Finally, the clusters in bath mode (B) dissociate with rate constant k_3 . A schematic description of this model is drawn in Fig. 9.

B. Effect of H-bond strength on the IVR and dissociation rate constants

In Table I, we first notice that the IVR rate constant k_1 correlates very well with the H-bond strength. The lifetime reduction of the OH stretching vibration upon H-bond formation is well known in the condensed phase and the present

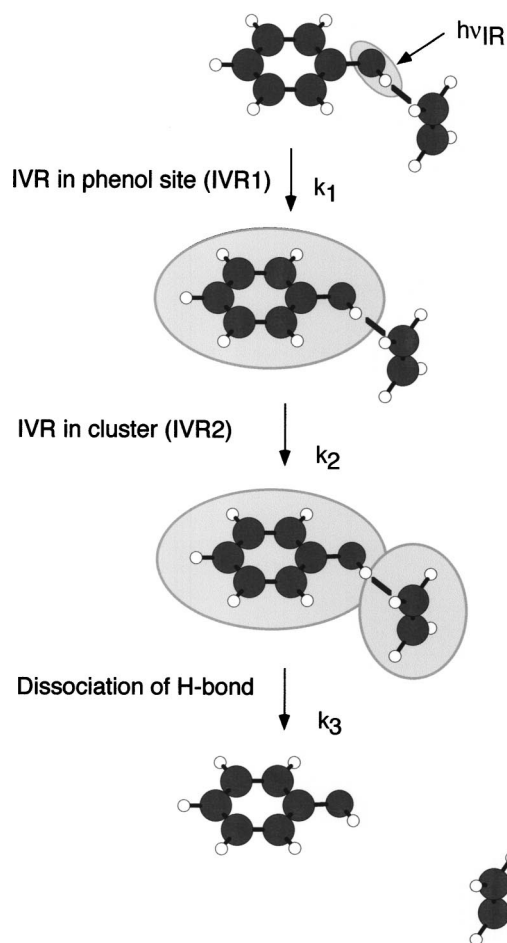


FIG. 9. Schematic diagram of the energy flow from the IR excitation to the OH stretching vibration to the dissociation of the H bond.

result essentially agrees well with the condensed phase observation. There have been many experimental results and theoretical treatments of the enhancement of the vibrational relaxation of the OH stretch upon H bonding, and the present results provide us with a new insight into its mechanism: *The H bonding is mostly effective in accelerating the redistribution of the OH stretch energy into intramolecular vibrational modes.*

Several candidates can be listed as the effective bath state for acceleration of the IVR of the OH stretch. First is the state(s) involving the CH stretching vibrations. In paper I, we showed that in bare phenol the OH stretch is strongly coupled to the levels involving the CH stretch vibration, leading to a rapid IVR of the OH stretch vibration. This coupling strength will be enhanced upon H-bond formation because of the following reasons: (1) The energy mismatch between the OH stretch level and the levels involving CH will decrease by H-bonding, resulting in a stronger anharmonic coupling because of the propensity rule⁴³ that the anharmonic coupling between states with smaller quantum number change should be larger. (2) In the H-bonded cluster, the combination between the CH and H-bonding intermolecular modes will be an additional effective bath state for the IVR of the OH stretch. Very recently, Wang *et al.* investigated the vibrational relaxation of the OH stretching vibra-

TABLE II. Vibrational frequencies (cm^{-1}) of intermolecular mode of hydrogen-bonded clusters of phenol used in the RRKM calculation. These frequencies are obtained by *ab initio* calculations with the MP2/6-31G level.

Mode No.	Phenol-ethylene	Phenol dimer	Phenol-DME
1	15.0	9.9	17.3
2	21.3	27.3	21.9
3	33.1	34.3	42.9
4	78.2	71.6	73.3
5	91.4	82.9	86.0
6	119.0	136.1	147.9

tion of ethanol liquid and found a very fast IVR into the symmetric stretching mode of the CH_2 group.¹² Though the present system is different from them, the observed result essentially agrees with their observation.

Another candidate for the effective bath state for the IVR of the OH stretch is the level(s) involving the overtone of the OH bending mode. The coupling between the H-bonded OH stretch and the first overtone of the OH bending mode is well known in water and alcohols as Fermi resonance and there are many theoretical treatments.⁴³⁻⁴⁸ In the present case, however, the frequency of the OH bending mode in phenol- d_0 and phenol- d_5 is $\sim 1170 \text{ cm}^{-1}$ (Ref. 49) so that there is large energy gap between the OH stretch and first overtone of the OH bend. Even if it is so, we cannot neglect this candidate because phenol- d_5 , having no CH oscillator, also exhibited substantial enhancement of the IVR rate of the OH stretch upon H bonding.

A further noticeable point in Table I is that the H-bond dissociation rate constants are very similar among the clusters in spite of the large differences in the binding energies. Since H-bond dissociation takes place after the IVR, it is quite interesting whether the dissociation takes place after complete energy randomization within the clusters. So we calculated the dissociation rate constants by using RRKM theory. In this theory, the dissociation rate constant is given by

$$k(E) = G^\ddagger(E - D_0) / h\rho(E). \quad (2)$$

Here $\rho(E)$ is the density of states of the cluster at the total energy of E and $G^\ddagger(E - D_0)$ is the number of possible states of fragments at an available energy of $E - D_0$, where D_0 is the H-bonding energy. The density of states was obtained by the direct counting method without taking account of anharmonicity. For phenol, C_2H_4 , and DME, most of their vibrational frequencies were taken from the literature. The vibrational frequencies which were not available in the literature were obtained by *ab initio* calculations with the MP2/6-31G level. The frequencies of intermolecular modes of the clusters were also obtained at the same level of the calculation, which are listed in Table II. For the H-bonding energy (D_0), we assumed those of the σ and π type to be 2100 cm^{-1} and 1100 cm^{-1} , respectively, by comparison of the experimental and theoretical values of other H-bonded clusters.^{36-40,50} The calculated dissociation rate constants k_{RRKM} are also listed in Table I. We also calculated the H-bond dissociation rate constant of phenol dimer, which is also compared with the experimentally obtained one. As seen in Table I, the agreement

between the observed and calculated rate constants is very poor. The RRKM calculation predicts a much larger dissociation rate constant for phenol-C₂H₂ than the phenol-DME and phenol dimer, while the observed rate constants are not so different among the clusters. The large discrepancy between the observed and RRKM calculated rate constants indicates that the dissociation of the H bond occurs much faster than complete energy randomization. Such a non-RRKM behavior of the dissociation is reported in many molecular clusters,⁵¹ and the present result will be an additional example of the non-RRKM behavior of the dissociation of the clusters.

V. CONCLUSION

The dynamics of the OH stretching vibration has been investigated for phenol H-bonded clusters by time-resolved picosecond IR-UV pump-probe spectroscopy. The results strongly indicate the importance of the “OH stretch↔intramolecular mode” coupling in the IVR of the H-bonded OH stretch. We found that in all clusters the initially excited phenolic OH stretching vibrational energy is primarily redistributed into the phenolic moiety, generating a hot phenol. Then the energy of the hot phenol flows into the intermolecular mode, followed by the dissociation of the H bond. Among them, the first step is strongly accelerated by the H bonding while others do not show a clear dependence on the H-bond strength. Finally, the H-bond dissociation rate constants do not agree with those calculated by the statistical theory, indicating that the energy is not fully randomized before dissociation.

ACKNOWLEDGMENTS

The authors wish to thank to Dr. A. Fujii, Dr. H. Ishikawa, and Dr. T. Maeyama for their helpful discussions. This work is supported by a Grant-in-Aid for Scientific Research (Grant No. 15350002) by J.S.P.S.

- ¹E. J. Heilweil, M. P. Casassa, R. R. Cavanagh, and J. C. Stephenson, *J. Chem. Phys.* **85**, 5004 (1986).
- ²H. Graener, T. Q. Ye, and A. Laubereau, *J. Chem. Phys.* **90**, 3413 (1989).
- ³H. Graener, T. Q. Ye, and A. Laubereau, *J. Chem. Phys.* **91**, 1043 (1989).
- ⁴H. Graener and G. Seifert, *J. Chem. Phys.* **98**, 36 (1993).
- ⁵S. Woutersen, U. Emmerichs, and H. J. Bakker, *J. Phys. Chem. A* **107**, 1483 (1997).
- ⁶A. J. Lock, S. Woutersen, and H. J. Bakker, *J. Chem. Phys. A* **105**, 1238 (2001).
- ⁷A. J. Lock and H. J. Bakker, *J. Chem. Phys.* **117**, 1708 (2002).
- ⁸R. M. Stratt and M. Maroncelli, *J. Phys. Chem.* **100**, 12981 (1996).
- ⁹J. C. Deak, S. T. Rhea, L. K. Iwaki, and D. D. Dlott, *J. Phys. Chem. A* **104**, 4866 (2000).
- ¹⁰L. K. Iwaki and D. D. Dlott, *J. Phys. Chem. A* **104**, 9101 (2000).
- ¹¹D. D. Dlott, *Chem. Phys.* **266**, 149 (2001).
- ¹²Z. Wang, A. Pakoulev, and D. D. Dlott, *Science* **26**, 2201 (2002).
- ¹³N. E. Levinger, P. H. Davis, and M. D. Fayer, *J. Chem. Phys.* **115**, 9352 (2001).

- ¹⁴K. J. Gaffney, I. R. Piletic, and M. D. Fayer, *J. Phys. Chem. A* **106**, 9428 (2002).
- ¹⁵R. Laenen and C. Rauscher, *Chem. Phys. Lett.* **274**, 63 (1997).
- ¹⁶R. Laenen, C. Rauscher, and A. Laubereau, *Chem. Phys. Lett.* **283**, 7 (1998).
- ¹⁷R. Laenen, C. Rauscher, and K. Simeonidis, *J. Chem. Phys.* **110**, 5814 (1999).
- ¹⁸S. Tanabe, T. Ebata, M. Fujii, and N. Mikami, *Chem. Phys. Lett.* **215**, 347 (1993).
- ¹⁹T. Ebata, T. Watanabe, and N. Mikami, *J. Phys. Chem.* **99**, 5761 (1995).
- ²⁰A. Iwasaki, A. Fujii, T. Ebata, T. Watanabe, and N. Mikami, *J. Phys. Chem.* **100**, 16053 (1996).
- ²¹T. Watanabe, T. Ebata, S. Tanabe, and N. Mikami, *J. Chem. Phys.* **105**, 408 (1996).
- ²²A. Mituzuka, A. Fujii, T. Ebata, and N. Mikami, *J. Phys. Chem. A* **102**, 9779 (1998).
- ²³Y. Matsuda, T. Ebata, and N. Mikami, *J. Chem. Phys.* **110**, 8397 (1999).
- ²⁴S. Ishikawa, T. Ebata, and N. Mikami, *J. Chem. Phys.* **110**, 9504 (1999).
- ²⁵N. Guchhait, T. Ebata, and N. Mikami, *J. Am. Chem. Soc.* **121**, 5705 (1999).
- ²⁶Y. Matsuda, T. Ebata, and N. Mikami, *J. Phys. Chem. A* **105**, 3475 (2001).
- ²⁷S. Y. Fredericks, K. D. Jordan, and T. S. Zwier, *J. Phys. Chem.* **100**, 7810 (1996).
- ²⁸F. C. Hagemester, C. J. Gruenloh, and T. S. Zwier, *Chem. Phys.* **239**, 83 (1998).
- ²⁹G. M. Florio, C. J. Gruenloh, R. C. Quimpo, and T. S. Zwier, *J. Chem. Phys.* **113**, 11143 (2000).
- ³⁰P. Tarakeshwar, K. S. Kim, and B. Brutschy, *J. Chem. Phys.* **110**, 8501 (1999).
- ³¹P. M. Palmer, Y. Chen, and M. R. Topp, *Chem. Phys. Lett.* **318**, 440 (2000).
- ³²E. G. Robertson, M. R. Hockridge, P. D. Jelfs, and J. P. Simon, *J. Phys. Chem. A* **104**, 11714 (2000).
- ³³Ch. Janzen, D. Spangenberg, W. Roth, and K. Kleinermanns, *J. Chem. Phys.* **110**, 9898 (1999).
- ³⁴B. Brutchy, *Chem. Rev.* **100**, 3891 (2000).
- ³⁵T. Ebata, M. Kayano, S. Sato, and N. Mikami, *J. Phys. Chem. A* **105**, 8623 (2001).
- ³⁶D. Feller, *J. Phys. Chem. A* **103**, 7558 (1999).
- ³⁷P. Tarakeshwar, K. S. Kim, S. Djafari, K. Buchholdm, B. Reimann, H.-D. Barth, and B. Brutchy, *J. Chem. Phys.* **114**, 4016 (2001).
- ³⁸D. B. Dupré and M. C. Yappert, *J. Phys. Chem. A* **106**, 567 (2002).
- ³⁹I. Vorobyov, M. C. Yappert, and D. B. Dupré, *J. Phys. Chem. A* **106**, 10691 (2002).
- ⁴⁰A. Courty, M. Mons, I. Dimmicoli, F. Piuzzi, V. Brenner, and P. Millié, *J. Phys. Chem. A* **102**, 4890 (1998).
- ⁴¹T. Ebata, M. Furukawa, T. Suzuki, and M. Ito, *J. Opt. Soc. Am. B* **7**, 1890 (1990).
- ⁴²M. Shatz, T. Bürgi, S. Leutwyler, and T. Fischer, *J. Chem. Phys.* **98**, 3763 (1993).
- ⁴³J. S. Hutchinson, W. P. Reinhardt, and J. T. Hynes, *J. Chem. Phys.* **79**, 4247 (1983).
- ⁴⁴A. Staib and J. T. Hynes, *Chem. Phys. Lett.* **204**, 197 (1993).
- ⁴⁵R. Rey and J. T. Hynes, *J. Chem. Phys.* **104**, 2356 (1996).
- ⁴⁶D. Chamma and O. Henri-Rousseau, *Chem. Phys.* **248**, 53 (1999).
- ⁴⁷D. Chamma and O. Henri-Rousseau, *Chem. Phys.* **248**, 71 (1999).
- ⁴⁸D. Chamma and O. Henri-Rousseau, *Chem. Phys.* **248**, 91 (1999).
- ⁴⁹H. D. Bist, J. C. D. Brand, and D. W. Williams, *J. Mol. Spectrosc.* **24**, 402 (1967).
- ⁵⁰J. L. Knee, L. R. Khundkar, and A. H. Zewail, *J. Chem. Phys.* **87**, 115 (1987).
- ⁵¹See, for example, T. Baer and W. L. Hase, *Unimolecular Reaction Dynamics: Theory and Experiments* (Oxford University Press, New York, 1996), pp. 369–415.